

The road to catastrophe: stability and collapse in 2D driven particle systems

M. R. D’Orsogna, Y. L. Chuang, A. L. Bertozzi, L. S. Chayes

Department of Mathematics, UCLA, Los Angeles, CA 90095 and

Department of Physics, Duke University, Durham, NC 27708

(Dated: October 17, 2018)

Understanding collective properties of driven particle systems is significant for naturally occurring aggregates and because the knowledge gained can be used as building blocks for the design of artificial ones. We model self propelling biological or artificial individuals interacting through pairwise attractive and repulsive forces. For the first time, we are able to predict stability and morphology of organization starting from the shape of the two-body interaction. We present a coherent theory, based on fundamental statistical mechanics, for all possible phases of collective motion.

PACS numbers: 05.65.+b, 45.50.-j, 45.40.Ln, 87.18.Ed

The swarming of multi-agent systems [1] is a fascinating natural phenomenon. The patterns formed by many self-assembling species pose a wealth of evolutionary [2] and biological [3, 4] questions, as well as structural and physical [5, 6, 7] ones. In more recent years, understanding the operating principles of natural swarms has also turned into a useful tool for the intelligent design and control of man-made vehicles [8, 9].

One of the main unresolved issues arising both in artificially controlled and biological swarms is the ability to predict stability with respect to size. If well defined spacings amongst individuals exist, swarm size typically increases with particle number, in a ‘crystal’ like fashion. This is generally true in animal flocks and might be a desirable feature in robotic systems. On the other hand, natural examples exist of swarms that shrink in size as particle number increases. For instance, in the early development of the *Mycococcus xanthus* or *Stigmatella auriantaca* fruiting bodies [10] two-dimensional bacterial vortices arise and grow until the vortices collapse inward, individual cells occupy the central core and a localized three dimensional structure appears. Although many swarming systems have been studied, and in some cases specific phase transitions have been observed [4, 7, 9], a systematic prediction of whether a swarm will collapse on itself or not as the number of constituents increases, has been lacking.

In this Letter, we apply fundamental principles from statistical mechanics to accurately predict the geometry and stability of swarming systems. Specifically, we consider N self-propelled particles powered by biological or mechanical motors, that experience a frictional force, leading to a preferred characteristic speed [11]. The particles also interact by means of a two-body generalized Morse potential. Previous related work [5], showed that in some cases localized vortices may form. Here, we explore the *entire* phase space defined by the interaction potential and predict pattern geometry and stability. The identical N particles obey the equations of motion:

$$m \frac{\partial \vec{x}_i}{\partial t} = \vec{v}_i, \quad (1)$$

$$m \frac{\partial \vec{v}_i}{\partial t} = (\alpha - \beta |\vec{v}_i|^2) \vec{v}_i - \vec{\nabla}_i U(\vec{x}_i), \quad (2)$$

with the generalized Morse potential given as:

$$U(\vec{x}_i) = \sum_{j \neq i} [C_r e^{-|\vec{x}_i - \vec{x}_j|/\ell_r} - C_a e^{-|\vec{x}_i - \vec{x}_j|/\ell_a}]. \quad (3)$$

Here, $1 \leq i \leq N$, and ℓ_a, ℓ_r represent the range of the attractive and repulsive part of the potential and C_a, C_r are their respective amplitudes. We remark that our analysis need not be confined to Morse-type potentials – these are simply a mathematical convenience. Combinations of other attractive and repulsive potentials lead to collective behaviors similar to those seen here. In particular, a similar analysis can be extended to the interactions of Ref. [7] and of Ref. [9], providing a much more complete prediction of stability.

In the special case of velocity independent forces, i.e. $\alpha = \beta = 0$, Eqns. 1-3 form a typical Hamiltonian system with a conserved energy. For a large number of particles, according to the ideas of statistical mechanics, the behavior of such a system should be described by a finite temperature (Maxwell-Boltzmann) distribution with the energy in the model determining the temperature [12]. A Maxwell-Boltzmann description is even more applicable when there is some mechanism for exchange of energy with the environment. Here, we argue that the parameters α and β in the model of Eqns. 1-3 provide a local mechanism for such energy exchanges. Thus, the gross features of our system should be described by a classical statistical mechanics model with the temperature parameter determined by α and β . Of course the detailed local behaviors, as well as the large scale collective dynamics, may be quite different – and ostensibly more interesting – than the corresponding system obeying Maxwell-Boltzmann statistics.

In large systems that obey the laws of statistical mechanics it is expected that thermodynamics will emerge as size and number of constituents tend to infinity. In order to ensure a smooth passage to the thermodynamic limit, the microscopic interactions must respect certain

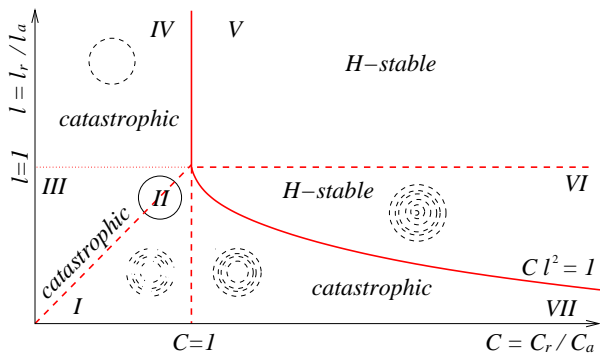


FIG. 1: H-Stability phase diagram of the Morse potential. The catastrophic regions correspond to parameter ratios $\ell = \ell_r/\ell_a$ and $C = C_r/C_a$ for which the thermodynamic limit does not exist. Extrema of the potential d_{min} exist only for $\ell > \max\{1, C\}$ and for $\ell < \min\{1, C\}$. In these cases $d_{min} = \ell_r \log(\ell/C)/(\ell - 1)$.

constraints. The most important of these is *H-stability*: for a set of N interacting particles, the potential energy U is said to be H-stable if a constant $B \geq 0$ exists such that $U \geq -NB$ [13]. This property ensures thermodynamic behavior, in particular that the N particles will not collapse as $N \rightarrow \infty$. Non H-stable systems are also called catastrophic. For Morse type interactions, conditions for H-stability are known. For example, if the d -dimensional integral of the potential is negative, the system is non H-stable. In this case, as N increases, the particles collapse into a dense body with energy per particle proportional to N . On the other hand, for thermodynamic systems, the energy per particle will be asymptotically constant. The stability phase diagram of the Morse potential is shown in Fig. 1. As we shall see the H-stability or lack thereof is instrumental in predicting the behavior of swarming systems obeying the likes of Eqns. 1-3.

For the full model, we numerically integrate Eqns. 1-3 using a fourth order Adams-Bashforth method [14] for free boundaries, effectively allowing an infinite range of motion for the particles. Initial conditions are chosen with localized particles and random velocities. The resulting behavior is consistent with the stability or catastrophic predictions of Fig. 1. We discuss system behavior in each region of the phase diagram of Fig. 1.

In the case $\min\{C, \ell\} < 1$ the interparticle potential is of catastrophic nature and globally attractive. For $\beta \neq 0$, particles tend to sustain a constant speed $|\vec{v}_i|^2 \sim \alpha/\beta$, while subject to attractive forces. This competition leads to non-equilibrium configurational patterns. We distinguish three subregions in the $\min\{C, \ell\} < 1$ region: $\{\ell < C\}$, $\{\ell = C\}$ and $\{\ell > C\}$, respectively regions I, II and III of Fig. 1. In region I a potential minimum d_{min} exists and the N particles self-organize by creating multi-particle clumps. Within each clump the particles travel parallel to each other defining a collective direc-

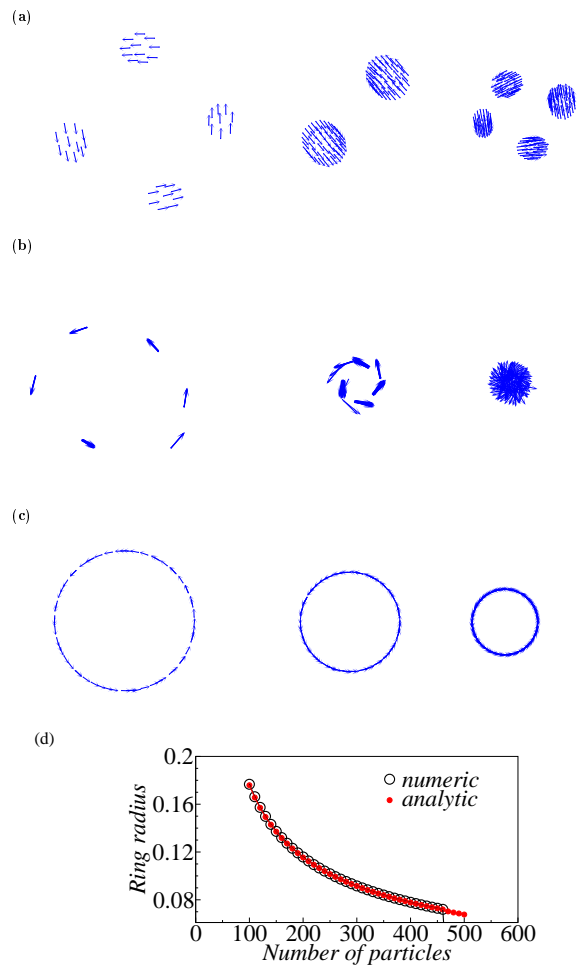


FIG. 2: Catastrophic geometry. (a) *Clumps*. From left to right $N = 40, 100, 150$. Clumps coalesce as N increases. The set parameters are $\alpha = 1, \beta = 0.5, C_a = \ell_a = 1, C_r = 0.6, \ell_r = 0.5$. (b) *Ring clumping*. From left to right $N = 40, 100, 200$. Parameters are the same as in Fig. 2a, but $\ell_r = 1.2$. (c) *Rings*. From left to right $N = 60, 100, 200$. Parameters are the same as in Fig. 2a, but $C_r = 0.5$. (d) Ring radius as a function of N from numerical data and Eq. 4. Parameters are the same as in Fig. 2c. Fitting data from Eq. 4 yields $R \sim N^{-0.52}$.

tion. Because of the rotational velocity, this direction changes in time and the clumps rotate about their center of mass (Fig. 2a). Catastrophic behavior is evident in the fact that as N increases, the clumped structures shrink instead of swelling. Interparticle distance also becomes smaller and eventually, as $N \rightarrow \infty$ clumps lose their coherence and merge. The bisectant $\{\ell = C\}$, region II, is the borderline for the existence of extrema. Here, the potential minimum occurs for $d_{min} = 0$, no associated finite length scale exists, and rings are developed (Fig. 2c). Assuming equidistant particle spacing, the ring radius R may be estimated by balancing the centrifugal and centripetal forces. An approximate implicit expression for

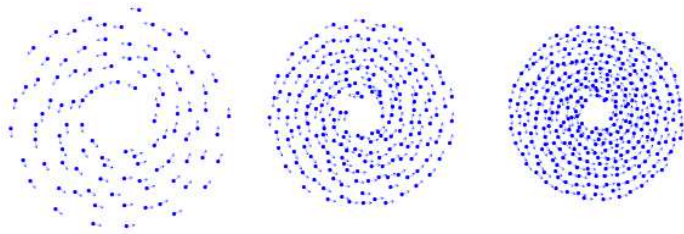


FIG. 3: Snapshots of swarms for different values of N in the catastrophic regime defined by region VII of Fig. 1. From left to right $N = 100, 200, 300$. Note the decrease in the vortex area and the dramatic density increase. The chosen parameters are: $C_a = 0.5, C_r = 1, \ell_a = 2, \ell_r = 0.5$. Self-propulsion and friction are fixed at $\alpha = 1.6$ and $\beta = 0.5$.

R is given by:

$$\frac{\alpha}{2R\beta} = \sum_{n=1}^{N/2} \sin\left(\frac{\pi n}{N}\right) \left[\frac{C_a}{\ell_a} e^{-\frac{2R}{\ell_a} \sin\left[\frac{\pi n}{N}\right]} - \frac{C_r}{\ell_r} e^{-\frac{2R}{\ell_r} \sin\left[\frac{\pi n}{N}\right]} \right] \quad (4)$$

Estimates of R as given by Eq. 4 match extremely well those obtained numerically as seen in Fig. 2d. Circular structures are also seen in the swarms of Ref. [15]. For $\{\ell > C\}$ in region III of Fig. 1, clumped structures appear although there is no minimum in the potential. In particular, no intrinsic interparticle spacing exists and the clumps consist of superimposed particles traveling along a ring: this type of collective motion is energetically more favorable than uniform spacing among particles. An example of ring clumping is shown in Fig. 2b.

A clumped ring structure also appears in the $\{C < 1 < \ell\}$ regime of region IV. The observed behavior is very similar to what described in the $\{\ell > C\}$ case above, with the difference that here the potential defines a maximum, and for low particle numbers the extra constraint of avoiding energetically costly interparticle spacings has to be considered. Region V of Fig. 1 where $\max\{\ell, C\} > 1$ corresponds to the H-stable regime. Here, the interparticle potential is characterized by overall repulsive behavior and is minimized by infinite separation. Thus, as $N \rightarrow \infty$ the particles will tend to occupy the entire volume at their disposal. The entire region is a ‘gaseous’ phase with particle speed peaked at $|\bar{v}_i|^2 = \alpha/\beta$.

The most interesting region of the phase diagram is defined by $\{\ell < 1 < C\}$, regions VI and VII of the phase diagram. Here, the potential is characterized by short range repulsion and long range attraction. A potential minimum exists and defines a length scale d_{min} . The $C\ell^2 = 1$ curve of Fig. 1 parts the thermodynamically stable region VI from the thermodynamically catastrophic region VII. Although the main features of the two-body potentials are similar, different H-stability properties lead to very different self-organizational behaviors in the moderate and large particle limits.

Region VI with $\{1/\sqrt{C} < \ell < 1\}$ corresponds to ther-

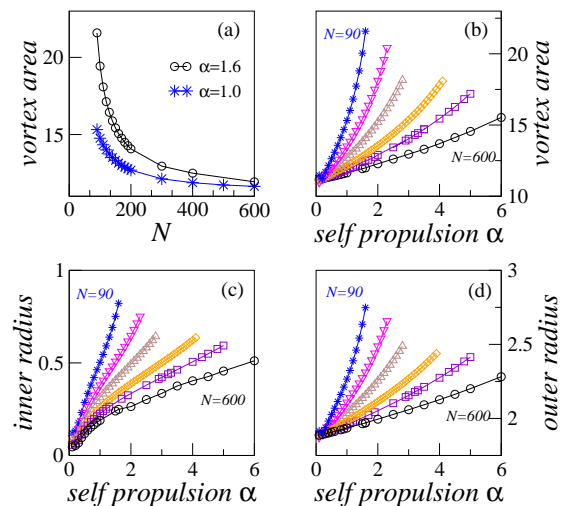


FIG. 4: Vortex scalings for the catastrophic Morse potential. The parameters are set as in Fig. 3. The friction term $\beta = 0.5$. (a) Vortex area as a function of N for $\alpha = 1.0, 1.6$. Note the dramatic decrease with N . (b) Vortex area as a function of (a) for various N . From top to bottom $N = 90, 140, 200, 300, 400, 600$. For any fixed α the vortex area decreases with N . (c) Inner and (d) Outer radii of the catastrophic vortices as a function of α . The particle numbers are the same as in Fig. 4b. Both radii increase with α but decrease with N . For large N the inner core disappears.

modynamic stability. At finite N , and for various values of α/β , particles approach the characteristic velocity $|\bar{v}_i|^2 = \alpha/\beta$ and reach a kinetic energy much greater than the confining interaction potential. The swarming agents tend to disperse as individuals. For much smaller values of α/β , the N particles assemble into organized structures with well defined spacings, which in the large particle limit tend to a finite value. Particles will then either swarm coherently in a rigid disk aggregate or flock with a finite center of mass velocity, depending on the initial conditions. In both cases, the motion is rigid body-like and interparticle distances are preserved. For $\alpha/\beta \rightarrow 0$, the particles assemble into static, locally crystalline structures.

Region VII where $\{\ell < 1/\sqrt{C} < 1\}$, corresponds to thermodynamic instability; all cases examined in Ref. [5] concern this region. As in the previous case, for finite N , large values of α/β will lead to a gaseous phase and very small values to crystalline structures whose motion is rigid body-like. However, quite unlike the H-stable scenario discussed above, these structures are unstable with respect to particle number, and in the $N \rightarrow \infty$ limit will collapse. At intermediate values of α/β , vortex structures appear with particles traveling close to the characteristic speed $|\bar{v}_i|^2 \sim \alpha/\beta$. Here, vortex size *decreases* dramatically as a function of particle number as seen in Figs. 3, 4. Also, for finite N , vortices rotating counter-clockwise and clockwise may coexist, depending

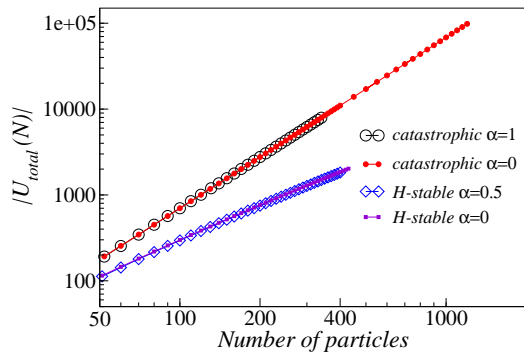


FIG. 5: Absolute value of the total Morse potential energy, $|U_{total}|$, as a function of N . Several choices of α are shown with fixed $\beta = 0.5$. The upper curves correspond to the catastrophic regime with the same Morse parameters as in Fig. 3. The scaling law is $-U_{total} \sim N^{2.0}$ for both $\alpha = 1$ and $\alpha = 0$. The lower curves correspond to the H-stable parameters $C_a = 0.5, C_r = 1$ and $\ell_a = 2, \ell_r = 1.5$. The scaling law is $-U_{total} \sim N^{1.0}$ for both $\alpha = 0$ and $\alpha = 0.5$. Scaling is linear in the H-stable case, and quadratic in the catastrophic one.

on the initial conditions. In this regime, the occurrence of double spiraling is visually most dramatic since it occurs within vortices, however double spiraling is a feature of the entire catastrophic part of the phase diagram and co-existing left and right direction of motions for clumped or equispaced rings occur as well. Double spirals are thus a strong indication of the non H-stable nature of the potential. Another typical feature of the catastrophic regime is that energy per particle does not asymptotically reach a constant value. This is seen in Fig. 5 where, in the non H-stable regime, the total energy scales quadratically, so that energy per particle grows linearly. Here, interparticle separation (not shown) decreases dramatically as $N \rightarrow \infty$. For comparison, in the H-stable regime, the total potential energy scales linearly with N and energy per particle does approach a constant. Likewise, as $N \rightarrow \infty$ interparticle separation is asymptotically constant.

The observed swarming behavior of *M. xanthus* is consistent with the catastrophic regime VII of the Morse potential where core free vortex structures can arise. The absence of a hard component for the interparticle interaction is justified by the fact that *M. xanthus* cells can penetrate each other by crawling. We propose the following qualitative and coarse scenario for the initial stages of aggregation. As the number of constituents increases, so does particle speed $\sqrt{\alpha/\beta}$. This is consistent with the observed enhancement of C-signal activity among particles [16] that increases motility. The bacterial vortex then increases its size with N and double spirals may coexist, as reported in the literature [17]. Eventually, bacterial speed reaches an upper limit and increasing N will lead the vortex to collapsed behavior, until, finally, it evolves into a complex 3D structure [18] due to finite

height of the cells and other features not accounted for in Eqns.1-3.

Simple modeling of interacting particles combined with thermodynamic reasoning can account for complex and subtle phenomena in biological systems. Furthermore, in spite of its name, the existence of a catastrophic regime might be of great benefit to the development of unmanned vehicle technology for the added versatility it offers. ‘Soft core’ robot interactions could be implemented by specialized cooperations at short distances e.g. robots crawling over or rotating about each other or by setting parameters so that actual individual size is minuscule compared to relevant length scales. For large or even moderate number of vehicles the programming of a crossover from an H-stable to a catastrophic regime could lead the robots to change from a dispersive (searching) behavior to convergence at a specified site.

We thank H. Levine and D. Marthaler for useful discussions. We acknowledge support from ARO and NSF through grants W911NF-05-1-0112 and DMS-0306167.

-
- [1] S. Camazine *et al.*, *Self organization in biological systems* (Princeton Univ. Press, Princeton, 2003); I. Prigogine, *Order out of chaos*, (Bantam, New York, 1984).
 - [2] J. K. Parrish and L. Edelstein-Keshet, *Science* **284**, 99 (1999); S. A. Kaufmann, *The origins of order: self-organization and selection in evolution* (Oxford Univ. Press, Oxford, 1993).
 - [3] I. D. Couzin, J. Krauss, N. R. Franks, S. A. Levin, *Nature* **433**, 513 (2005); I. Riedel, K. Kruse, J. Howard *Science* **309**, 300 (2005); G. Flierl, D. Grünbaum, S. A. Levin, D. Olson, *J. Theor. Biol.* **196**, 397 (1999).
 - [4] I. D. Couzin, J. Krause, R. James, G. D. Ruxton, N. R. Franks, *J. Theor. Biol.* **218**, 1 (2002).
 - [5] H. Levine, W. J. Rappel and I. Cohen, *Phys. Rev. E*, **63**, 017101 (2000).
 - [6] J. Toner and Y. Tu, *Phys. Rev. Lett.* **75**, 4326 (1995); W. Ebeling and U. Erdmann, *Complexity* **8**, 23 (2003); T. Vicsek, A. Czirak, E. Ben-Jacob, I. Cohen and O. Shochet, *Phys. Rev. Lett.* **75**, 1226 (1995); E.V. Albano, *Phys. Rev. Lett.* **77**, 2132 (1996); G. Grégoire, H. Chaté, *Phys. Rev. Lett.* **92**, 025702 (2004);
 - [7] A. Mogilner, L. Edelstein-Keshet, L. Bent and A. Spiros, *J. Math. Biol.* **47**, 353 (2003).
 - [8] E. Bonabeau, M. Dorigo and G. Theraulaz, *Swarm intelligence: from natural to artificial systems* (Oxford Univ. Press, Oxford, 1999); N. E. Leonard and E. Fiorelli *Proc. 40th IEEE Conf. Decision and Control*, 2968 (IEEE, Orlando, 2001).
 - [9] V. Gazi and K. Passino, *IEEE Transactions on Automatic Control* **48**, 692 (2003).
 - [10] A. L. Koch and D. White *Bioessays* **20**, 1030 (1998); S. Kim and D. Kaiser *Science* **249**, 926 (1990).
 - [11] R. Hilborn *Chaos and Nonlinear Dynamics* (Oxford Univ. Press, Oxford, 2001).
 - [12] K. Huang, *Statistical Mechanics* (Wiley, New York, 1987).
 - [13] D. Ruelle, *Statistical Mechanics, Rigorous results*, (W. A. Benjamin, Inc., New York, 1969).

- [14] G. H. Golub and James M. Ortega *Scientific Computing and Differential Equations: An Introduction to Numerical Methods* (Academic Press, New York, 1992).
- [15] W. Ebeling, F. Schweitzer, *Theor. Biosci.* **120**, 207 (2001).
- [16] L. Jelsbak and L. Sgaard-Andresen, *Proc. Nat. Acad. Sci.* **99**, 2032 (2002).
- [17] O. A. Igoshin, R. Welch, D. Kaiser and G. Oster *Proc. Nat. Acad. Sci.* **101**, 4256 (2004); K. A. O'Connor and D. R. Zusman *J. Bacteriol.* **171**, 6013 (1989).
- [18] J. M. Kuner and D. Kaiser, *J Bacteriol.* **151**, 458 (1982); D. Kaiser, *Nature Reviews Microbiology* **1**, 45 (2003).